Relativistic laser nano-plasmonics

A.Andreev[1,2,3], K.Platonov[4] , J.Braenzel[1,6], A.Lübcke[1], S.Das[1], H.Messaoudi[1], R.Grunwald[1], C.Gray[5], E.McGlynn[5], M.Schnürer[1]

[1] Max-Born Institute, Berlin, Germany

[2] ELI-ALPS, Szeged, Hungary

[3]Sankt Petersburg State University, St. Petersburg, Russia

[4] State Technical University, St. Petersburg, Russia

[5]School of Phys. Sci., National Centre for Plasma Science and Technology, Dublin, Ireland
[6]Technical University Berlin, Straße des 17. Juni 135, 10623 Berlin, Germany

Abstract

Particle acceleration and X-ray generation in different nano-structured targets irradiated by high intensity laser pulses of high contrast have been studied. It is found that maximal energy of fast particles and its directionality can be significantly enhanced, by choosing nano-structured targets. Generation and propagation of fast electrons in laser targets consisting of nano-wires are studied. Such targets exhibit a large conversion of laser energy into electron kinetic energy. An electron bunch can propagate a long distance and can be focused by bringing wires together. The results of theory and simulations were compared with the experimental data and have shown a reasonable consistency.

Introduction

Laser driven nano-plasmonics deals with optical processes in plasmas at relatively low intensities and on nanoscale, i. e. on the order of or smaller than the wavelength of the laser radiation [1]. The underlying physical process is connected with a laser field enhancement due to proper nano-structuring of a target. Laser-matter interaction including nanoscale confinement of radiation and its transformation provides attractive opportunities for both, fundamental research and technological applications. Material processing uses femtosecond laser pulses exceeding the material ablation threshold to drill micro holes, to realize micro cutting or to selectively remove a particular substance. Such an extreme precision processing adds high value [2]. Due to the ultrashort pulse durations the results benefit by very clean and defined processing areas with negligible structural changes around. This is important in surgery (e. g. ophthalmology, dermatology, dentistry), for instance, when the ultrashort laser pulse irradiation enables clean surgery without damaging the side areas of the processed tissue [3].

Laser nano-plasmons produced by structured surfaces have recently gained growing attention in laser plasma ion acceleration physics, as it can significantly enhance the acceleration mechanism. Today's research on laser driven particle acceleration (ions and electrons) promises future fast ion sources for different applications. Here, a laser at relativistic intensity interacts with thin solid foils, which can be well characterized and easily handled [4]. First, the laser causes an acceleration of the ionized electron distribution, which subsequently accelerates ions up to high kinetic energies. The low emittance of such ion beams is a striking feature [5]. Nevertheless, up to now the achieved acceleration efficiency is low (around a few to ten percent of the laser energy), even if the target thickness is optimized with respect to the laser parameters, thus current research is focusing on its optimization [6].

It is obvious, that surface modification acts back on the light absorption in general. Hence, the combination of nanostructuring with high field laser interaction promises an enhancement of the efficiency. A key question concerns the development of the nanostructure during the high intensity laser irradiation and what consequences follow. This implies a direct connection between laser and target parameters and its restrictions, which are studied and discussed in this paper.

In the following, interaction of an ultra high intensity and high temporal contrast ($<10^{-10}$) laser pulse with different nanostructured targets is studied. Special emphasis is paid to consequences of the generation of fast ions. It is found that their maximum energy and directionality can be significantly enhanced by choosing targets with a specific nanostructured surface. Under optimum conditions the absorption of laser energy can be close to 100%. In this case, the conversion of laser energy into fast ion energy can approach several ten %. Our theoretical and simulation results show a reasonable agreement with the experimental data obtained by different classes of surface nanostructures.

Formation of nanostructures by femtosecond laser

Recent theory predicts a new class of meta structures by engineered sub-wavelength entities, which enable unprecedented properties for electro-magnetic radiation. These specific structures do not exist in nature [1] and will have profound impact on integrated nano photonics. As an example, the realization of a so-called super lens that focuses far below the diffraction limit, can be mentioned.[2]

Considering practical applications, easy-to-handle and cost-effective methods for surface structuring using different materials are desirable. One of the most convenient top down approaches is the formation of laser-induced periodic surface structures (LIPSS) [7], which are regarded as a self-organizing mechanism. It exploits the interference of the incoming light wave with a secondary wave (scattered light or a surface plasmon wave generated in the material [8]) and its propagation along the surface [9]. At high intensities and broadband excitation as delivered by ultrashort-pulse lasers, the scenario becomes more complex by including multiphoton excitation channels and/or spectral selectivity. As shown for different types of materials like, e.g. W [10], Si [11], TiN [12] or diamond-like carbon [13], nonlinear excitation with femtosecond laser pulses enables structural periods well below the excitation wavelengths (sub-wavelength LIPSS). For the formation of such nanoscale LIPSS (nanoripples) in dielectric media, two distinct types of structures are observed, which can be described as ablation reliefs (see, e.g., [12]) or the creation of deep, nearly planar grooves or nanoplanes normal to the surface. Extended-area structuring on fixed and moving substrates was obtained by applying line focusing with a cylindrical lens. Under defined conditions with respect to pulse number, pulse energy and scanning velocity, two types of ripple-like LIPSS with high and low spatial frequencies corresponding to periods in the range of 90 nm and 340 nm, respectively, were formed [13].

Additionally, another class of nanostructures with significantly smaller structural width has been studied. ZnO nanorods were grown on a Ti foil by chemical bath deposition on drop coated seed layers. Here, a mixture of equal volumes of 0.02 M zinc nitrate and 0.8 M NaOH solutions at 70°C for 25 minutes was applied. Further details of these methods are described in [14,21].

Interaction of intense short laser pulse with nanostructured targets

Absorption

Experimental and theoretical investigation of laser driven ion acceleration determined a significant enhancement for the fast ions in terms of maximum energy and flux if thin foils are used as the laser irradiated target. Nevertheless, the absorption of the laser light does not exceed the 50% level [15]. An ideal target would combine maximum absorption and

minimum mass, which can be realized with thin substrate foil covered by long, nano cylinders, i. e. a so-called brush target [16]. The absorption of laser energy in such a target reaches up to 100% and the conversion of laser into ion energy can approach tens of percent [17]. In the following, we analyze the efficiency of the interaction of grating-like nanostructures on a robust foil target (foil thickness above 1 micron) with an ultra intense laser pulse.

In our simulations we investigate a substrate foil of few hundred nanometer thickness at solid density. An imposed relief structure on front and rear side is characterized with different ledges. The parameters of the rectangular ledge at the front side are denoted as: d_1 - width, d_2 - distance between the ledges, h - ledge height and the thickness of the substrate foil as *s*, cf. Fig.1. The parameters of the relief at the rear side are subscribed just as those at the front side but with capital letters.

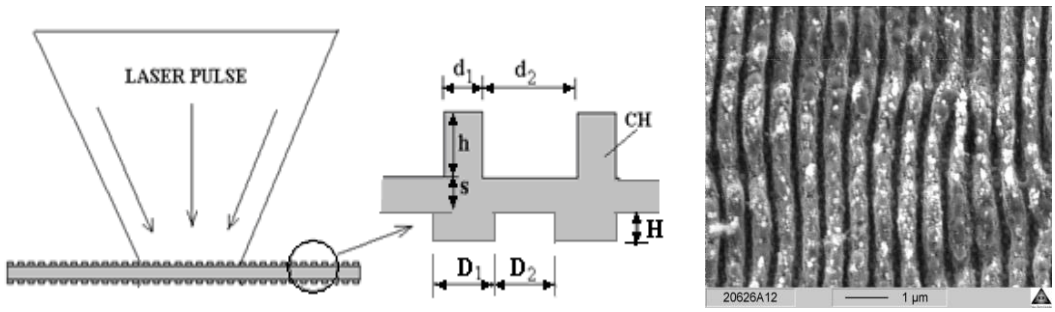

Fig.1 Schematic of the nanostructure target and example of a laser induced ripple structure

We also varied the density of ion constituents, i.e. heavy ions are C^{+6} and light ones are H^{+1}. Protons can be additional deposited as a thin layer on the rear surface. The purpose of target parameter optimization is to achieve both, a high absorption of the laser pulse in the target and the maximum energy of the accelerated ions.

Simulation model

The investigation is based on 2D particle in cell (PIC) modelling of the motion of plasma particles. With the help of the modified code PSC, the modelling was performed for different targets. In 2D simulations with our PIC code [6] we used the following parameters: a laser wavelength of $\lambda_L = 0.8\,\mu m$, intensity values of I_L=(0.5, 1, 5) 10^{20} W/cm^2, pulse durations of t_L=15, 30 fs and a spot size d_L=3 μm. The simulations have been performed in a simulation box of 100x100 μm^2 divided into 5x10^7 cells with 30 particles of each type in a cell.

It was shown [18] that in case of a target with a non-structured rear side the electric field at the rear side has a regular profile. Contrary, at the structured front side, the field reproduces a relief distribution. Thus, the quality of the accelerated proton beam differs for each side. We will now consider only the rear side component.

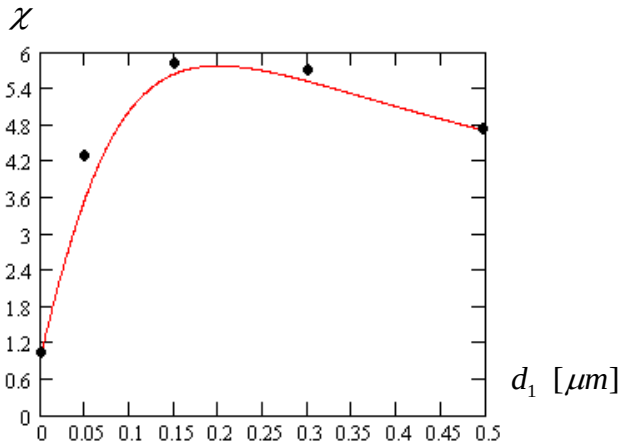

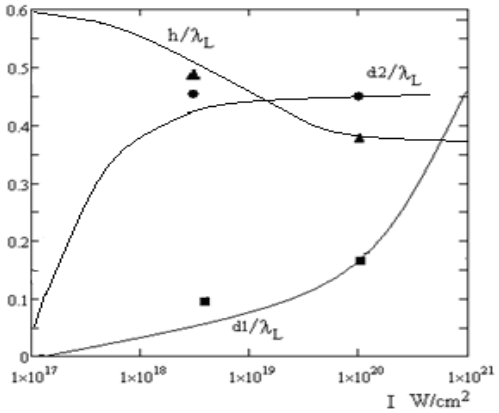

a) b)

Fig.2 a) The factor of absorption enhancement χ in relation to plane foil absorption as a function of parameter d_1 at h = 0.4 μm, s = 0.3 μm, d_2 = 0.35 μm and I =10^{20}W/cm^2; b) Optimum structure parameters (in relation to laser wavelength) of a rectangular front relief as a function of the laser intensity at t_L=30 fs and the spot size d_L=3 μm. The solid lines are the results of analytical model and black squares, cycles and triangles show the optimal parameters d_1, d_2, h obtained from PIC simulations.

In Fig.2a black dots represent the absorption enhancement in relation to plane foil absorption as a function of parameter d_1 as observed in the simulations. It is seen from Figs. 2a that the optimal relief enhances the absorption of laser energy by a factor of 6 at laser intensity 10^{20}W/cm^2.

Analytical model

To explain these dependencies we developed an analytical model based on our previous work [18,19]. The laser field E_L acting on the surface of the relief with an orientation perpendicular to the laser polarization (simply called lateral surface with its normal vector parallel to the electric field vector) is capable of taking electrons into vacuum from an maximum extraction depth of $l_{extr} = E_L / en_e$, where n_e is the electron density in the skin layer and e is the electron charge. Therefore, $d_1 \geq 2l_{extr}$ should be fulfilled. The number of electrons leaving the unit area of the relief at optimum conditions is $dN_e / dS = n_e d_1 / 2 = \frac{(d_1 / 2l_{extr})}{\sqrt{1+(d_1 / 2l_{extr})^2}} E_L / e$. The total lateral surface, from which electrons leave, is $S = hd_L[2d_L / (d_1 + d_2)]$, where d_L is the laser spot-size. The characteristic size of an electron orbit near the relief is $r_{eh} = CeE_L / m_e\omega_L^2$, where $C \sim 1$ (for a single electron in vacuum C=1, but the influence of other electron decreases C). Therefore, the optimum distance between the two ledges of the relief can be written as, $d_2 = 2r_{eh}$. Accordingly, the maximum electron energy in vacuum can be estimated for an optimum profile as: $\varepsilon_{tot} = \frac{(d_1 / 2l_{extr})}{\sqrt{1+(d_1 / 2l_{extr})^2}} \frac{(d_2 / 2r_{eh})\sqrt{2}}{\sqrt{1+(d_2 / 2r_{eh})^2}} (hd_L / e)[2d_L E_L / (d_1 + d_2)]\varepsilon_{eh}$,

where m_e is the electron mass, ω_L is the laser frequency, $\varepsilon_{eh} = m_e r_{eh}^2 \omega_L^2 / 2$. Then, the relative absorption is given by:

$$\chi = \begin{cases} 1 + \frac{(d_1 / 2l_{extr})}{\sqrt{1+(d_1 / 2l_{extr})^2}} \cdot \frac{(d_2 / 2r_{eh})}{\sqrt{1+(d_2 / 2r_{eh})^2}} \cdot \frac{2h}{(d_1 + d_2)} \cdot \frac{4\pi r_{eh}}{ct_L}, & \chi \leq \chi_{\max} \\ \chi_{\max}, & \chi > \chi_{\max} \end{cases} \qquad (1)$$

Here $\chi_{\max}$ is the relative absorption for the optimum relief when the laser energy $\varepsilon_L \approx \varepsilon_{tot}$ which corresponds to simulations (cf. Fig.2a). With (1) the dependency χ on parameter d_1 is calculated and plotted with a solid line in Fig. 2. A good agreement with simulation results has been obtained for C=0.6.

In the following we consider the influence of the rear side relief on the parameters of accelerated particles. It was shown [18] that only at the front side of the target the ambipolar electric field reproduces a relief distribution. Thus, hot electrons have a quasi-equilibrium state in the ion field and can be described with the help of a density distribution at an effective temperature because of electron re-circulations in a thin foil. Therefore, the influence of the front relief is described by varying the temperature and

density of hot electrons. Laser pulse parameters are taken into account via expansion of a relativistic electron gas inside the target and its relevant parameters. During acceleration, the laser irradiated target expands, and the parameters of the electron gas obey the adiabatic law, $p_e / n_e^{\gamma} = T_{e0} / n_{e0}^{\gamma-1}$ where p_e and n_e are the pressure and density of hot electrons, respectively, and T_{e0} and n_{e0} are the initial values of their temperature and density. Since the acceleration time of ions is longer than the traveling time of a relativistic electron through the target, we can neglect the inertia of electrons in the hydrodynamic equation of motion. We write the condition of local equilibrium of the electron gas as $e\partial\varphi / \partial\vec{r} = -n_e^{-1}\partial p_e / \partial\vec{r}$, where φ is the scalar potential of the ambipolar field in the target. Using the adiabatic law of expansion of the electron gas, we can easily express the electron density from the balance equation of forces in terms of the potential as follows:

$n_e(\varphi) = n_{e0}\left(1 + \frac{\gamma-1}{\gamma}\frac{e\varphi}{T_{e0}}\right)^{\frac{1}{\gamma-1}}$. We choose the adiabatic index as γ = 2 in line with a 2D geometry in PIC - simulations. Therefore, the two-dimensional Poisson equation for the potential and the field that accelerates ions becomes linear $\Delta\varphi = -4\pi|e|[Zn_{1i}(y,z) + n_{2i} - n_e(\varphi)]$ and can be solved for the relief target. The density of the positive heavy ions for the rear relief (see Fig.1) can be written as

$$\mathrm{n_{1i}(y,z) = n_{1i0}\sum_k \theta(y - k(D_2 + D_1))\theta(kD_2 + (k+1)D_1 - y)\cdot\theta(H/2 - |z|) + n_{1i0}\theta(-H/2 - z)\theta(z + H/2 + s)}$$

where $\theta(z)$, $\theta(y)$ are step functions. The density of light ions $\mathrm{n_{2i0}} << \mathrm{n_{1i0}}$ is described as an ultrathin layer at the surface of relief (contamination thickness $s_2 << D_1$):

$$\mathrm{n_{2i}(y,z) = n_{2i0}\sum_{k=-\infty}^{\infty} \delta(y - k(D_2 + D_1))\delta(kD_2 + (k+1)D_1 - y)\cdot\theta(H/2 - |z|) +}$$
$$\mathrm{+\theta(y - k(D_2 + D_1))\theta(kD_2 + (k+1)D_1 - y)\cdot\delta(H/2 - z) +}$$
$$\mathrm{+\theta(k(D_2 + D_1) - y)\theta(y - (k-1)D_2 - kD_1)\delta(-H/2 - z)}$$

Let us introduce the dimensionless potential $\psi = e|\varphi|/T_{e0}$ and normalize the coordinates $\xi = y / d_2$ (along the target surface), $\varsigma = z / h$ (perpendicular to the target surface) and the time to the ion plasma frequency $\tau = \omega_{pi}t$, $\omega_{pi}^2 = 4\pi Z^2 n_{1i0} e^2 / m_i$. In dimensionless variables, the Poisson equation for the dimensionless density of hot electrons, which scales linearly with the potential $\psi = 2(\eta_e - 1)$, takes the following form:

$$\mathrm{2(\rho^2\frac{\partial^2}{\partial\xi^2} + \mu^2\frac{\partial^2}{\partial\varsigma^2})\eta_e = \eta_0\eta_e - \sum_k \theta(\xi - k(1 + D_1/D_2))\theta(k + (k+1)D_1/D_2 - \xi)\cdot\theta(1/2 - |\varsigma|) +} \quad (1)$$
$$\mathrm{+\theta(-1/2 - \varsigma)\theta(\varsigma + 1/2 + s/H)}$$

here $\mathrm{r_D^2 = T_{e0}/4\pi e^2 Z n_{1i0}}$, $\eta_0 = n_{e0}/Zn_{1i0}$, $\rho = r_D / d_2$, $\mu = r_D / h$.

The equation of proton motion can be written in the following form:

$$\frac{\partial^2\varsigma}{\partial\tau^2} = -\frac{2\mu^2}{\eta_0}\frac{\partial\eta_e}{\partial\zeta} \qquad \frac{\partial^2\xi}{\partial\tau^2} = -\frac{2\rho^2}{\eta_0}\frac{\partial\eta_e}{\partial\xi}, \quad (2)$$

Since $\mathrm{n_{2i0}} << \mathrm{n_{1i0}}$ protons are considered as test particles moving in the field of heavy ions and hot electrons. The linear differential equation (1) was solved with help of a 2D Fourier transformation.

The potential inside the relief forms a saddle with a convex structure along the z-axis and a weakly concave structure along the «y» direction. Owing to this saddle shape, the light ions starting inside the relief are squeezed towards the central axis at ξ=0.5 (cf. Fig.3a) slide

down the potential surface and being finally ejected out of the structure. The numerical solution of the equation of ion motion (Eq. (2)) in the potential (Eq.(1)) is shown in Fig.3a.

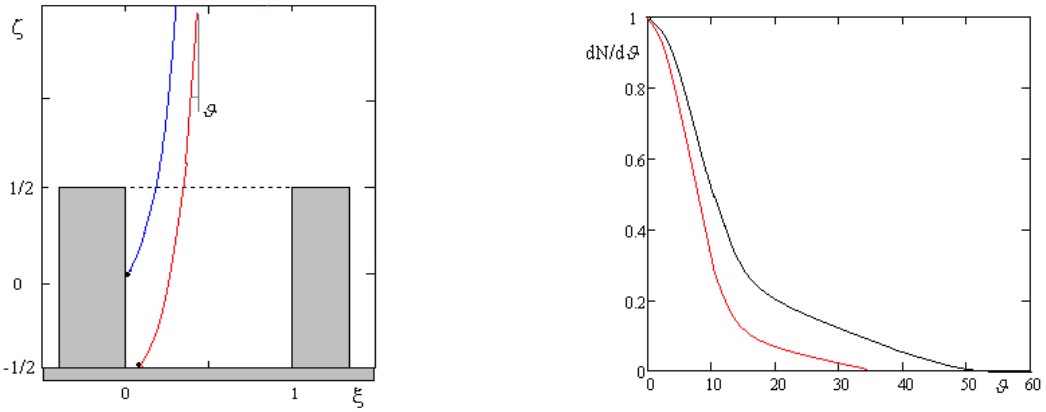

a) b)

Figure 3 a) The proton trajectories with different initial position $\varsigma_0 = -0.5$, 0.05 and $\xi_0 = 0.1$, 0.0 in the potential ψ, $D_1 / D_2 = 0.3$; b) the proton angle distribution function for $D_1 = 100nm$, $D_2 = 540nm$, $H = 200nm$, $n_{e0} = 8 \cdot 10^{20} cm^{-3}$, $n_{1i0} = 6 \cdot 10^{22} cm^{-3}$, $T_{e0} = 6.5\, MeV$ (black line), $D_1 = 100nm$, $D_2 = 1000nm$, $H = 200nm$ (red line).

The proton trajectory is determined by its initial position (ξ_0, ς_0) in the thin surface layer (Fig.3a). The number (per unit length) of protons accelerated from the lateral relief surface in Fig.3a and located in the interval $d\varsigma_0$ is $dN = n_{2i0} s_2 H d\varsigma_0$, $\varsigma_0 \in [-0.5; 0.5]$, $\xi_0 = 0,1$. The number of protons accelerated from the horizontal surface located in the interval $d\xi_0$ is

$$dN = n_{2i0} s_2 D_2 d\xi_0, \quad \begin{cases} \xi_0 \in [0;1], & \varsigma_0 = -0.5, \\ \xi_0 \in [1; 1 + D_1 / D_2], & \varsigma_0 = 0.5 \end{cases}$$

Dividing this number by the angular interval $d\vartheta$ (ϑ - is the proton emission angle, see Fig.3a), one can get $dN / d\vartheta$, thus the parametric dependence (parameters ξ_0, ς_0) of the proton angular distribution function is as follows:

$$\frac{dN}{d\vartheta} = n_{2i0} s_2 H / \left| \frac{d\vartheta(\varsigma_0)}{d\varsigma_0} \right| + n_{2i0} s_2 D_2 / \left| \frac{d\vartheta(\xi_0)}{d\xi_0} \right|, \quad \begin{cases} \vartheta = \vartheta(\varsigma_0), & \varsigma_0 \in [-0.5; 0.5], \ \xi_0 = 0,1 \\ \vartheta = \vartheta(\xi_0), & \xi_0 \in [0;1], \ \varsigma_0 = -0.5, \\ \vartheta = \vartheta(\xi_0), & \xi_0 \in [1; 1 + D_1 / D_2], \ \varsigma_0 = 0.5 \end{cases} \qquad (3)$$

From (3) it is obvious that the maximum of the angular distribution is at $d\vartheta(\xi_0) / d\xi_0 \approx 0$, $\xi_0 \sim 0.5$ (see Fig.3a) and therefore we find its maximum at θ~0. In Fig.3b the distribution (3) is represented by a black solid line for the following parameters: $D_1 = 100nm$, $D_2 = 540nm$, $H = 200nm$, $n_{e0} = 4 \cdot 10^{20} cm^{-3}$, $n_{1i0} =, 6 \cdot 10^{22} cm^{-3}$ $T_{e0} = 7\, MeV$ and by red line for: $D_1 = 100nm$, $D_2 = 1000nm$, $H = 200nm$. The temperature and density of hot electrons are taken from numerical simulations (see below). From Fig.3b one can see that the increase of the distance between ledges at the rear side decreases the angular distribution of protons.

To check our model we performed 2D PIC simulations with the same parameters for the rear structure but we used front side ripples with h = 0.4 μm, d_2 = 0.35 μm, d_1 = 0.15 μm. The thickness of the $Ti^{+20}H^{+1}$ target was 300 nm. Laser parameters were: I_L=10^{20} W/cm^2, duration t_L=30 fs and the spot size d_L=3 μm. Angular and spectral characteristics of accelerated protons are given in Fig.4, obtained with and without a relief.

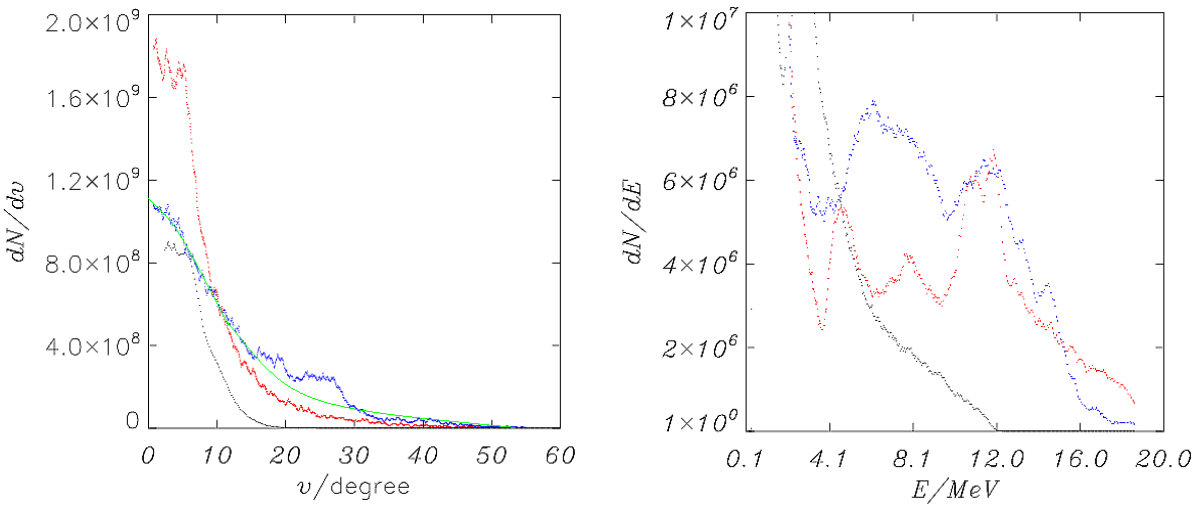

a) b)

Fig.4 a) Proton angular distributions for different targets b) Energy distribution of protons propagating at an angle $\pm 30^0$ with respect to the target normal. Plane foil – black color, foil with front relief – red, foil with front and rear reliefs – blue. Here h = 0.4 μm, s = 0.3 μm, d_2 = 0.35 μm; $D_1 = 0.1\,\mu m$, $D_2 = 1\,\mu m$, $H = 0.2\,\mu m$, $I = 10^{20}$W/cm^2, τ_L =30 fs, $d_L = 3\,\mu m$.

From Fig.4 one can deduce that the optimum front relief increases the number of protons about 2 times and the maximum energy about 1.6 times. The width of the angular distribution (~ 10°) is about the same as for the plane foil. The rear relief slightly increases this width by the additional side (lateral) surfaces. The number and maximum proton energy is the same as for the case of the front relief (see Fig.4b). Anyway, the rear relief significantly increases the number of protons at high kinetic energies (4 -16 MeV) as it has a larger surface providing an enhanced ambipolar field for proton acceleration.

Stability of the relief structures during the laser-foil interaction

It is apparent from these results that relief structures play an important role in laser absorption and in consecutive particle acceleration. Hence, it becomes necessary to study if these relief structures are preserved during the full interaction time with the high intensity laser pulse. We divide the investigation of the relief stability into two parts: first we consider the case where the target does not move in the laser pulse direction and second, when the target is accelerated in laser propagation direction. For a stationary target, the pre-pulse of the main laser pulse can destroy the surface modulation due to heating and subsequent pre-plasma formation. It is possible to estimate the laser pre-pulse duration, which is not detrimental for the surface modulation, i. e. at which the spatial extent of the ion thermal wave is smaller than the spacing between the ledges. The intensity of the pre-pulse corresponds to the experimentally achievable contrast. Estimation of absorption at a certain contrast level and following target expansion translates into a restriction for the pre-pulse duration. In case of light target material typically a duration of ns is derived. Replacement of carbon by heavy material can increase the tolerable pre-pulse duration up to several nanoseconds.

The ponderomotive pressure of the laser pulse can also deform the relief, when electrons are pushed deeply inside the target. The resulting strong electrostatic field causes deformation of the target surface if the laser intensity approaches ~ 10^{21} W/cm^2 for our target parameters [18].

The question of limitation by the pulse duration is also very important. In Fig. 4 the spatial distribution of the relief is shown at different times. Evidently, after the ion expansion from the initial distribution a new dynamic structure was created exhibiting a maximum density at the positions of previous minima. This dynamically formed new relief persists sufficiently

long (~ 100 fs), and thus high absorption of incident laser light at very high intensity is possible even for several 100 fs, which makes this scheme interesting even for longer pulses. In order to approximate the dynamic lifetime of the relief we use the model concerning equations (1,2) and insert parameters d_1, d_2, h instead of D_1, D_2, H. Smoothing of a relief (increase of d_1) can be interpreted as the motion of its vertical (lateral) boundary in the potential $\psi(\xi, \varsigma = 0)$ (cf. Fig.3a). The motion of relief boundaries obeys the period conservation $d_1(t) + d_2(t) = d_{10} + d_{20} = d_0$. A relief reproduces itself if $d_1 > d_{10} + d_{20}$ and new dense ledges appear. We associate the relief lifetime t_r with the time when $d_1(t_r) = d_{10} + d_{20}$. Considering the motion of potential boundaries of the relief, one can write the following formula for the relief lifetime:

$$\tau_r = \int_0^{1/2} \frac{d\xi}{\sqrt{2(\psi(\xi = 0, \varsigma = 0) - \psi(\xi, \varsigma = 0))}} \qquad (4)$$

The calculation (4) for the parameter of Fig.5 yields about 100 fs which is close to 70 fs when in Fig.5b the collision of ion fronts from side walls of the front relief are observed. The lifetime of this new structure (dynamic relief) is about 100 fs allowing an irradiation with pulses of several 100 fs duration.

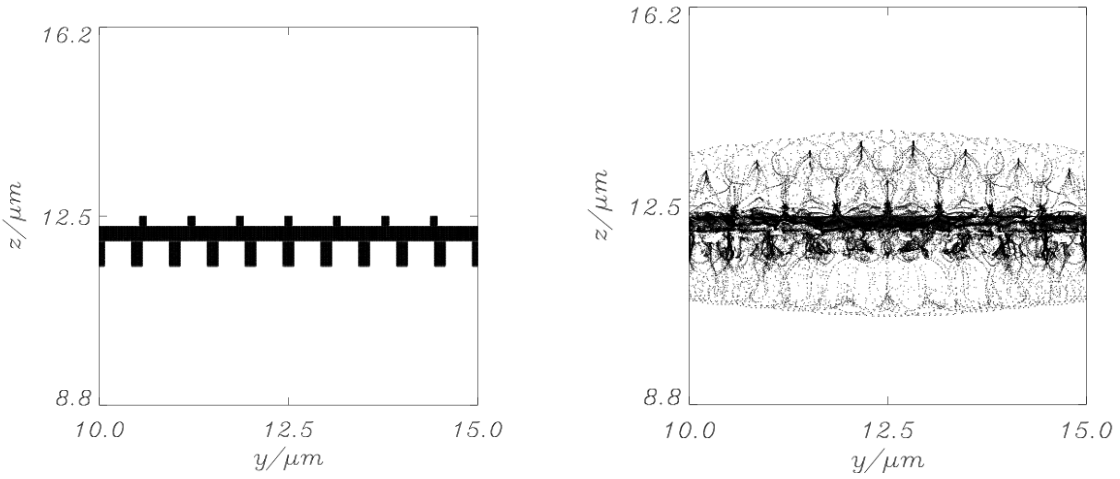

a) b)

Fig.5 a) The initial profile with a front- (down) and rear-side (up) relief of the target b) creation of the new dynamic relief when stagnation of ion fronts from side parts of the relief occurs at t=69 fs after interaction of a 30 fs laser pulse. The laser and target parameters are shown in Fig.4.

Fast particle generation

Now, after having studied target dynamics, the maximum proton energy attainable with nano relief targets will be investigated.

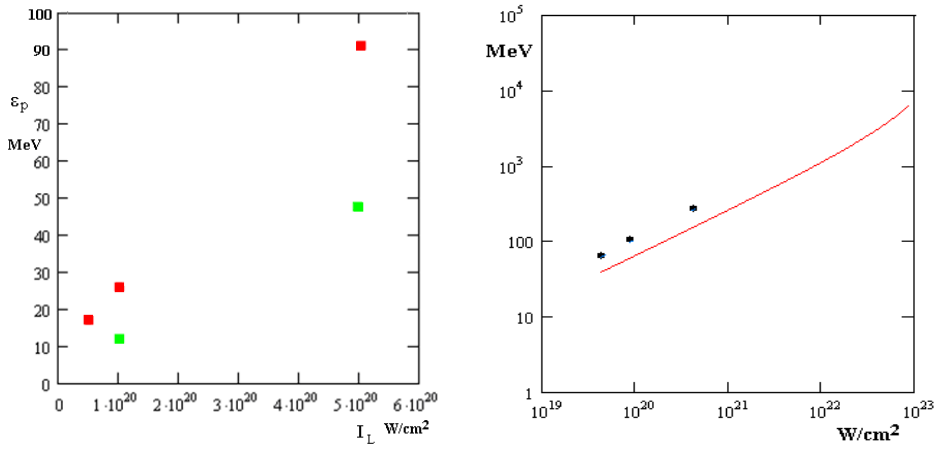

a) b)

Fig.5 a) Dependence of proton energy on laser intensity for optimum front relief (red squares): h = 0.4 μm, s = 0.3 μm, d_2 = 0.35 μm, d_1 = 0.15 μm for $5*10^{19}$, 10^{20} W/cm^2; h = 0.4 μm, s = 0.3 μm, d_2 = 0.4 μm, d_1 = 0.3 μm for $5*10^{20}$ W/cm^2 ; t_L=30 fs; green squares correspond to a plane foil of the same thickness b) Dependence of ion C^{+6} energy on laser intensity. Black dots are the maximal energies of carbon ions for optimally structured targets. The red line is the result of the formula (5) at $\alpha = 1$.

In Fig.5a the dependence of maximum proton energy (red squares) on the laser intensity is shown for optimum relief parameters. For comparison, the maximum proton energy for a plane foil is shown (green squares).
For an optimum relief and based on the simulation we derive scaling equations for the maximum energy (above 5 MeV) and the number of light and heavy ions:

$$\varepsilon_p \approx 17(I_L / 5\cdot 10^{19} Wcm^{-2})^{0.6}[MeV] \qquad N_p \approx 7\cdot 10^7 \cdot (I_L / 5\cdot 10^{19} Wcm^{-2})^{0.86}$$

$$\varepsilon_C \approx 69(I_L / 5\cdot 10^{19} Wcm^{-2})^{0.62}[MeV] \qquad N_C \approx 7.4\cdot 10^7 \cdot (I_L / 5\cdot 10^{19} Wcm^{-2})^{0.75}$$

The main part of the absorbed energy is transformed into kinetic energy of the heavy ion component ε_C . This energy component is calculated using energy and momentum conservation laws: in the lab frame one obtains

$$\varepsilon_C - m_i c^2 = \frac{2\varepsilon_L - F(I_L)}{N_C(I_L)} \frac{\left(2\varepsilon_L - F(I_L)\right)}{2m_i c^2 N_C(I_L) + 2\left(2\varepsilon_L - F(I_L)\right)} \qquad (5)$$

with R, η being the reflection and absorption coefficients, respectively, taking into account that for a nontransparent target $R + \eta = 1$. Incorporating simulation results we yield $N_C(I_L) = N_i (I_L / I_{cr})^{0.75}$, $I_L < I_{cr}$; $N_C(I_L) = N_i$, $I_L > I_{cr}$ where N_i is the total ion number in the laser spot. Here, the critical laser intensity [4] is $I_{cr} = cE_{0\,max}{}^2 / 4\pi = \pi c e^2 n_e{}^2 l_f{}^2$. The energy loss function describing the energy flux directed outward from the laser spot is:

$$F(I_L) = F_0 \cdot \left(\frac{I_{cr} - I_L}{I_{cr} - I_{0L}} \right)^{\alpha}$$, where $F_0 = 0.35\,10^{16}$ eV, $\alpha \approx 1$ and $I_{0L} = 10^{20} W / cm^2$ at $I_L \le I_{0L}$;

at $I_L > I_{0L}$, $F = 0$. The dependence $\varepsilon_C = \varepsilon_C(I_L)$ from (5) is shown in Fig.5b. Equation (5) describes average ion energies and explicitly not the maximum values. These values are quite similar in analytical and numerical calculations. At very high laser intensities (in the

order of 10^{21} … 10^{22} W/cm^2), in the so called "piston" regime, the absorption coefficient is close to unity and a surface structure does not provide any longer an advantage.

Transport of hot electron current

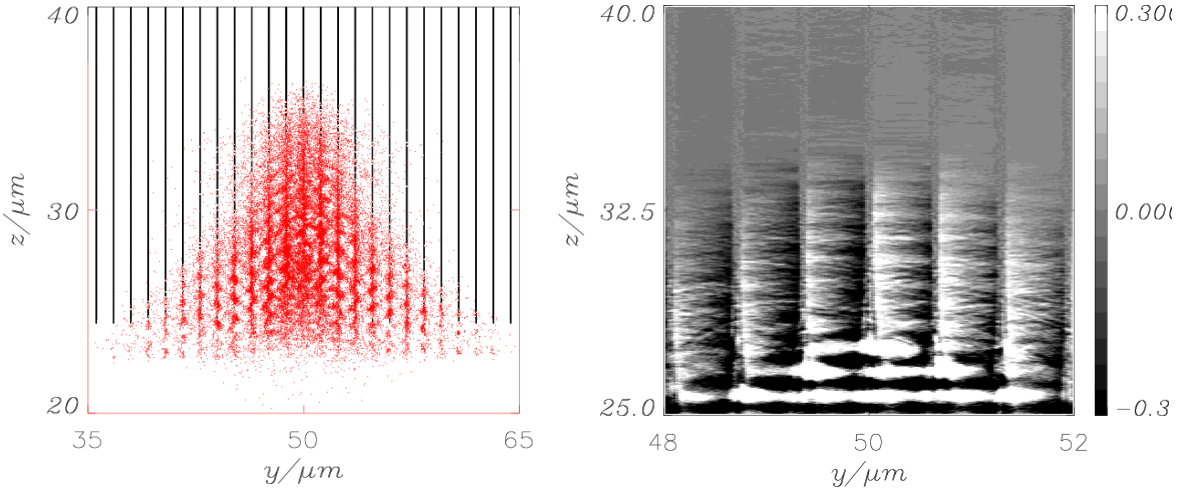

a) b)

Fig.6 a) Spatial distribution of hot electron density and b) Normalized electric field E_y/E_L due to propagation of fast electrons in a carbon wire target with wire diameter of 60 nm and a wire spacing of 650 nm. Laser pulse parameters are: d_L = 4 μm, duration of the Gaussian pulse 45 fs, intensity $I_L = 3\times10^{19}$W/cm^2. Distributions 65 fs after the start of interaction are shown. Laser hits the target from the bottom.

Transmission of high electron currents in targets is always accompanied by generation of cold return currents, which compensate self-generated magnetic fields of the beam. In dense targets such return currents lead to instabilities, filamentation of the relativistic current and turbulences. In targets of specific structures such processes can be mitigated, because the parameters of filamentation are known and the process may be suppressed with an appropriate transport structure. The goal is to extend significantly the propagation length of the relativistic electron beam. Present technologies allow engineering targets with a bundle of wires of nanometer diameter [20], which will not be destroyed by the laser pulse [6] with sufficient high temporal contrast. The motion of the hot electrons along the wire surface provides the opportunity to focus the electron beam, leading to an area of maximum density and correspondingly maximum energy density of hot electrons.

Our modelling was performed for a target consisting of parallel wires. The laser with 0.8 μm wavelength irradiates the edges of the wires parallel to their surface from the bottom. The focal spot diameter is d_L = 4 μm, duration of the Gaussian pulse is 45 fs, and the intensity is $I_L = 3\times10^{19}$W/cm^2. The target consists of carbon wires with diameter of $s \geq 40$ nm and a separation distance ≥ 100 nm. We found that in case of parallel wires, optimum conditions for number and energy of the hot electrons are fulfilled, if the target diameter is of the order of the skin layer l_s and the distance between the wires is about the Debye radius of the hot electrons. The simulation shows that in such targets a bunch of hot electrons can be created which propagates deeply into the target. In Fig.6a the propagation of the relativistic electron beam along the target wires and in Fig.6b the propagation of transversal component of electric field is shown. One can see, that the laser field does not propagate along the wires but it transforms into a surface wave propagating along the wires with a velocity close to the speed of light together with the relativistic electrons.

These results are in contrast to dense targets, where only very few hot electrons can reach comparable distances. The physical reason of extended hot electron propagation along the

wires is the generation of a return current of cold electrons in the wires: hot electrons which partly leave the wire cause a positive charge which attracts cold electrons in the surrounding wire volume. The density of the return current in the wire is larger than the hot electron current density in the wire, but both currents compensate each other if the hot electrons propagating in the vacuum interspace are added. Thus, the hot electron bunch can propagate along the wire over a remarkable distance. The analysis of the angular distribution of the hot electrons finds the maximum electron density within an angle of 10°. This means, while the electrons are propagating along the wire at the speed close to *c* they undergo transverse oscillations (three-dimensional spiral-like motion) in the electrostatic field of the wire which is termed "Debye wrapping" of the propagating electron bunch.

Experimental observations

Experiments have been performed at the Max Born Institute High Field Ti:Sapph laser. It delivers 1.3 J on target with pulse durations of (30−35) fs. Contrast enhancement by an XPW [20] frontend leads to a peak to ASE contrast of ~10^{11}. An ultra-short (< 100fs) pre-pulse at a level of 10^{-7} peak intensity precedes the main pulse by approximately 8 ns and is due to residual surface reflection inside the laser chain. Other experiments showed that this pre-pulse does not destroy or significantly heat a 30 nm thin polymer foil. The laser is focused by F/2.5 off- axis parabola mirror to a focal FHWM size of 4 µm, yielding a peak intensity of 6×10^{19} W/cm^2. We focused the laser on free-standing 5 µm thick Ti foil with different nano-structures. In the first case (cf. Fig.7a), a brush target of irregular structure was engineered by chemical bath deposition similar to [21]. In the second case, we used ripple targets, which have been prepared by laser induced periodic surface structuring (LIPSS) [14,22] using a separate kHz fs-laser.

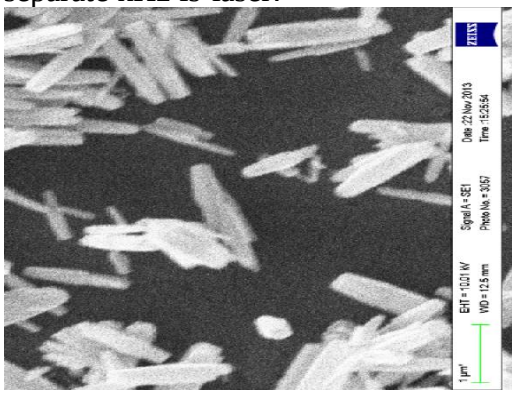

a)

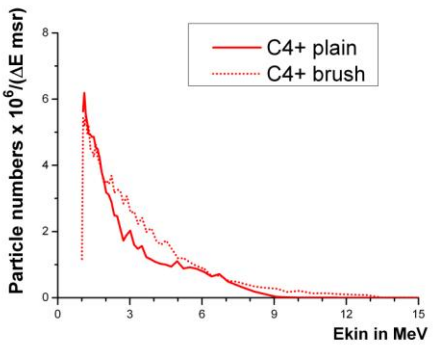

b)

Fig. 7 a) ZnO nanorods on 5 um Ti foil d_1=250nm, h>250nm b) Ion energy distribution

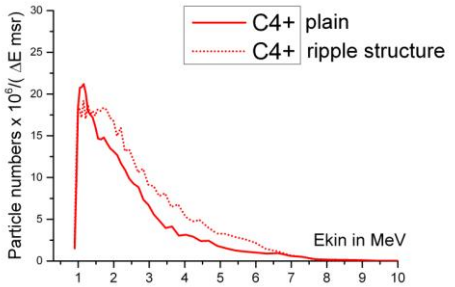

a)

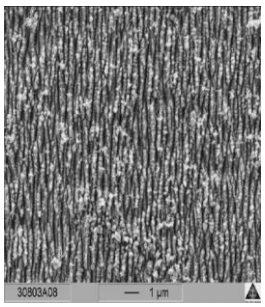

b)

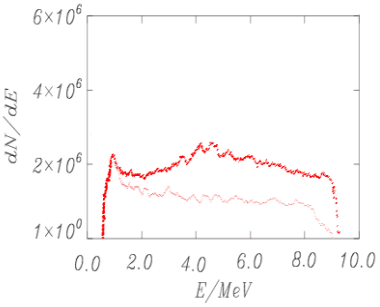

c)

Fig.8 a) The experimental ion energy distribution functions for the plane and ripple target at d_1=200nm, d_2=100nm, h=200nm b) The image of the ripple target c) The calculated ion

energy distribution functions for the plane (pink) and ripple (red) target from $Ti^{+15}C^{+4}$ at the front relief parameters: d_1=200nm, d_2=100nm, h=200nm. I_L= 6 10^{19}W/cm^2, t_L=30fs, d_L=4 μm.

The experimentally obtained energy spectral distribution of protons and carbon ions are displayed in Figs.7a and 8a for interaction with plane foil and nanostructured foil targets. It is clearly visible that the ion number is significantly enhanced for both structures in comparison to the plain foil case. The brush structure furthermore shows a small enhancement in the energy cutoff of C^{4+}, while the cut-off energy remains unchanged for the ripple structure. A parameter set close to the experiment has been used for the simulation in Fig. 8c, which yields similar spectral characteristics compared to the plain foil. The total energy ratio between plane and structured target of the experimentally measured ion spectra is determined to be ~1.4. In the simulation we calculated the total energy of C^{+4} ions correspondingly with $E_{tot} = \int E(dN/dE)dE$ and found that the ratio is $E_{tot}^{(ripple)} / E_{tot}^{(plain)} \approx 2.3$. The small difference is connected with the simulation geometry.

Conclusion

In summary, we have shown that a nano-relief structure with optimum parameters can significantly increase the short-pulse laser absorption, which is related to an enhancement of electron movement between relief ledges. A developed analytical model permits the approximation of the absorption enhancement in dependence on the relief parameters. The optimum relief height decreases with increasing laser intensity. But for the higher intensities the efficiency of such target stays high because here a transition to another dominant acceleration mechanism – the "laser piston" sets in. In the considered cases, degradation of the structure by a laser prepulse is crucial and a very high temporal contrast of the laser-pulse is required. The demand on an ultrashort laser pulse duration is relaxed, since after destruction of the original relief a secondary dynamic structure of ion density appears. Thus, strong absorption related to a plasma relief persists for a relatively long time of several hundred fs. This opens further options for the applications of structured targets. As an alternative approach a nano-wire target (very high relief) has been investigated permitting almost total absorption of the high intensity laser pulse, which later on is converted into a bunch of relativistic electron beams. They propagate along the nano-wires for a long distance (tens of mm). As these electron bunches can follow a denting of the wire they can be focused into a small spot. The presented experimental results confirm in particular the theoretically predicted enhancement of ion numbers from laser irradiated nano-structured targets. Further investigation concerning achievable maximum ion energies by additional target parameters (thickness, structure size) remains necessary.

References

1. Stockman M., OPTICS EXPRESS **19**, 22029 (2011)
2. Stockman M., Phys. Today **64**, 39 (2011)
3. Lal S.et al., Accounts Chem. Res., **41**, 1842 (2008)
4. Mourou G., Tajima T., Bulanov S., Rev. Mod. Phys., **78,** 309 (2006)
5. Fuchs J. et al., 25 December 2005; doi:10.1038/nphys199
6. Daido H. et al., Rep. Prog. Phys. **75**, 056401 (2012)
7. Andreev A., Steinke S., Schnuerer M. et al., PHYSICS OF PLASMAS **17**, 1 (2010)
8. Sipe J. E., Young J. F., Preston J. S. and van Driel H. M. *Phys. Rev.* B **27** 1141 (1983); Young J. F., Preston J. S., van Driel H. M. and Sipe J. E. *Phys. Rev.* B **27** 1155 (1983)

9. Kumagai H., Machida H., Toyoda K. and Tanaka S. *Japan. J. Appl. Phys.***30** 3186 (1991)
10. Kolasinski K. W. *Curr. Opin. Solid State Mater.Sci.* **11,** 76 (2007)
11. Zhao Q. Z., Malzer S. and Wang L. J. *Opt. Lett.* **32,** 1932 (2007)
12. Crawford T. H. R. and Haugen H. K. *Appl. Surf. Sci.* **253,** 4970 (2007)
13. Dufft D., Rosenfeld A., Das S. K., Grunwald R. and Bonse J., *J. Appl. Phys.***105** 034908 (2009)
14. Das S., Dasari K., Rosenfeld A. and Grunwald R., Nanotechnology **21** 155302 (2010)
15. Macchi A., Rev. Mod. Phys., **85**, 751 (2013)
16. Henig A., Steinke S., Sokollik T. et al., Phys. Rev. Lett. **103**, 245003 (2009)
17. Rajeev P.P., Banerjee S., Sandhu A.S. et al. , Phys. Rev. A **65**, 052903 (2002)
18. Andreev A., Kumar N., Platonov K., Pukhov A., PHYSICS OF PLASMAS **18**, 103103 (2011)
19. Andreev A.A. and Platonov K. Yu. Contrib. Plasma Phys. **53**, 173 (2013)
20. Kalashnikov M.P. et al., Proceedings of SPIE (2004)
21. Byrne D., E. McGlynn, K. Kumar, M. Biswas, M.O. Henry and G. Hughes, Crystal Growth Design,**10**, 2400 (2010)
22. Ostrikov K., REVIEWS OF MODERN PHYSICS, **77**, 489 (2005)

Acknowledgment

The research leading to these results has received funding from Deutsche Forschungsgemeinschaft within the program CRC/Transregio 18, and from LASERLAB-EUROPE (grants agreement n° 284464, EC's Seventh Framework Program). A.Andreev acknowledges funding from Deutsche Forschungsgemeinschaft within the project Nano-Plasma Photonik and the provided computation resources of JSC at the project HBU15.